Chapter 5

Measurement of scatter broadening of pulsars at 327 MHz

5.1 Introduction

Apart from the intrinsic variation of the pulse profiles emitted from pulsars which has been discussed in the previous chapters, the interstellar medium also affects the shape of the pulse (see chapter 1). The density fluctuations in the interstellar plasma are responsible for the scattering of radio waves, and this has been studied extensively ever since the discovery of scintillations in pulsars (Scheuer 1968). The scattering of pulsar signals can be studied through many observable effects like the temporal broadening of pulse profiles, angular broadening and scintillations (see Rickett 1990 and references therein). By studying these different effects one can hope to study the density fluctuations in the interstellar medium (for example, Alurkar, Slee & Bobra 1986; Gwinn, Bartel & Cordes 1993).

Out of the 706 pulsars listed in the pulsar catalogue by Taylor et al. (1993; updated version, 1995) the measured temporal broadening exists for only 145 pulsars. Hence a systematic survey for measuring the scatter broadening in a large number of pulsar directions where such data are not available yet, was undertaken by us using the Ooty Radio telescope (ORT). To help improve detailed study of the distribution of the free electron density in the Galaxy it is desirable that such measurements are available for a larger sample. For the first phase of our observations we selected 27 high dispersion measure pulsars. In section 5.3 we report the observations and discuss the results.

In the second phase, we selected pulsars in the direction of the Gum nebula to measure the scatter broadening in that direction. In section 5.4 we report the observations and results for 21 pulsars observed towards the Gum nebula and discuss the results.

5.2 Ooty Radio Telescope

The scatter broadening observations reported here were started in January 1996 using the ORT located in Southern India, situated at a latitude of about 11°N and longitude of 76" 40'E and at an altitude of 2150 meters above sea level. ORT has an offset-parabolic cylindrical reflector, whose dimensions are about 500 meters in North-South, and 30 meters in East-West and has an equatorial mount. The feed array consists of 1056 dipoles, grouped into modules with 48 dipoles per module, kept at the focus of the off-axis parabolic reflector (Swarup et al 1971, Sarma et al. 1975a, 197511, Kapahi et al. 1975) and oriented along North-South. The antenna is not sensitive to the other (East-West) component of polarisation. The telescope operates at a fixed centre frequency of 327 MHz with a bandwidth of about 16 MHz. The telescope is located on the slope of a hill with an inclination 11" to the horizontal plane. The slope is deliberately chosen to be equal to the latitude of the place, thus making a natural setting for the equatorial mount of the telescope. A source at the zenith can be tracked for about 9 hours (-4 to +5 hrs of Hour Angle) by moving the telescope in the east-west direction about its axis. Tlie declination range covered is $\pm 55°$ and can be achieved by phasing the array electronically.

In Fig 5.1, we show the block diagram of a module of the ORT. The output from each dipole is passed through a low-noise amplifier and a phase shifter and 48 such dipoles are combined in a Christmas tree fashion to form one module. There are 22 such modules –11 in the northern half and 11 in the southern half of the telescope. The signal from each module is down-converted to an intermediate frequency (IF)of 30 MHz by mixing with a local oscillator at a frequency of 296.5 MHz, after passing through a

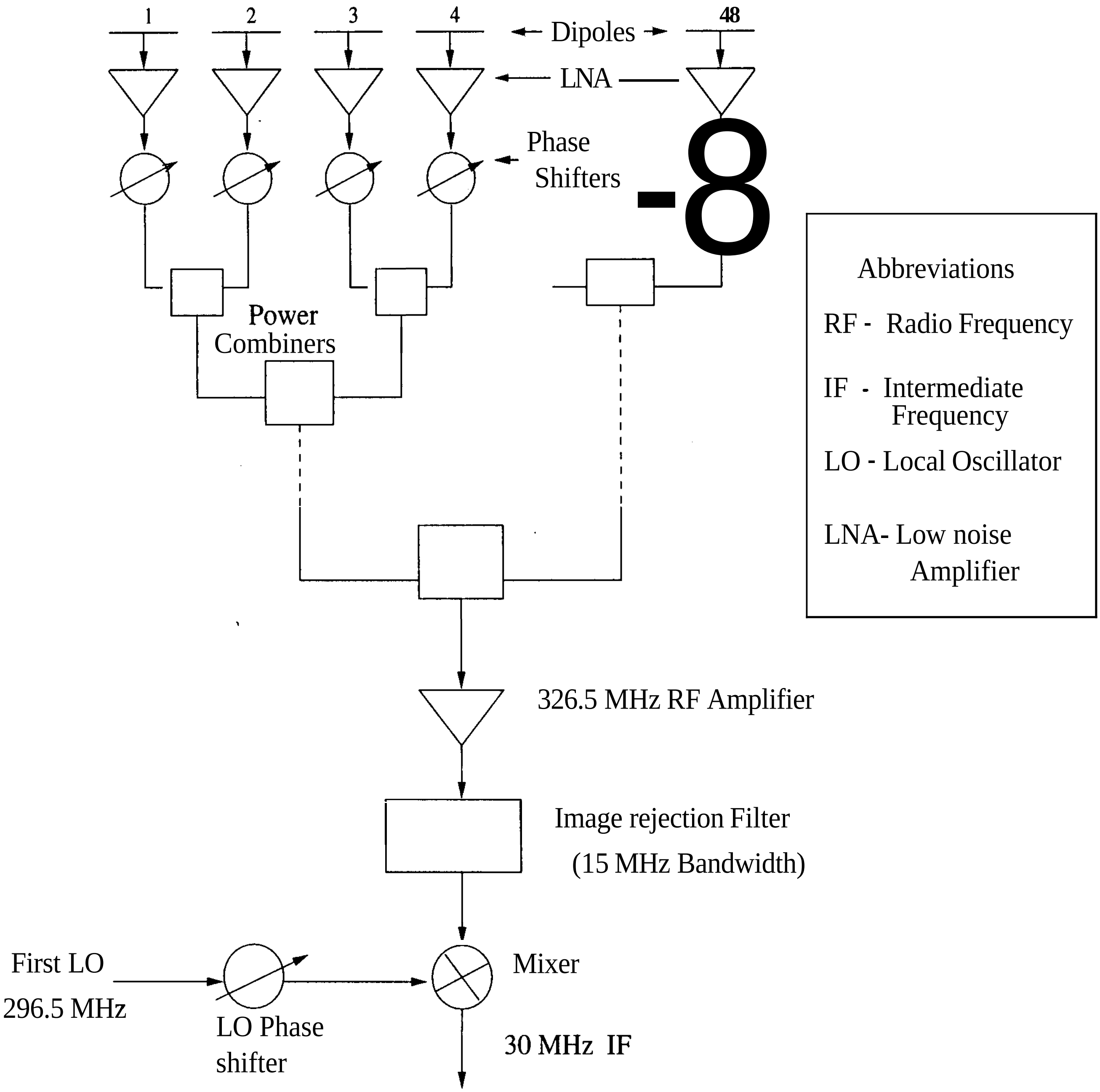

Figure 5.1: The block diagram of a module of the Ooty Radio Telescope.

radio frequency amplifier and an image rejection filter of 15 MHz bandwidth. The rest, of tlie front-end electronics is kept in the receiver room which is situated atljacent to the antenna. The delays due to the path difference between the modules are compensated by adjusting the lengths of cables in the signal path. Since the delay compensation is done at 30 MHz, a net phase difference remains which can be compensated in the local oscillator path. The IF signal is amplified by preamplifiers before and after the delay compensation. The delay compensated signal from each module is divided using a 12-way power splitter. The 12 sets of outputs from each of the 11 modules of the north side are combined with different phase gradients by a beam-forming-network to generate 12 beams around the specific direction. Similarly 12 beams are produced in the southern half. The 12 north and south beams are either added or correlated to get a total power or correlation beam respectively. The full width at half maximum (FWHM) of the total power and the correlation beam in the north-south direction are $5.5\sec(\delta)$ and $3.3\sec(\delta)$ arcmin respectively, where δ is the declination. The FWHM is 2° for both the correlated and the total power beams in the east-west direction. The 12 beams span about $\pm 18'$ around a specific declination and is separated by $3\sec(\delta)$ arcmin. For our observation we have mostly used the central (total power) beam and sometimes an adjacent beam, designated Beam 7 and Beam 5.

5.3 High DM pulsars

5.3.1 Observation

The IF signal is used as an input to a special purpose pulsar processor loaned to us by J. Ables and D. McConnell. This-processor passes the input signal through four filters, each of width 2.5 MHZ and spans a band of 10 MHz from 25 to 35 MHz. The signals from each of the filters are sampled using harmonic complex sampling at the Nyquist rate. Everv sample trains is then Fourier transformed to obtain 256 spectral channels across each of the 4 filters. Thus all the 1024 channels producetl has a fixed witltli of 10 kHz each. The channel outputs are detected in the total power mode and are digitally delayed to compensate for the interstellar dispersion, before adding them

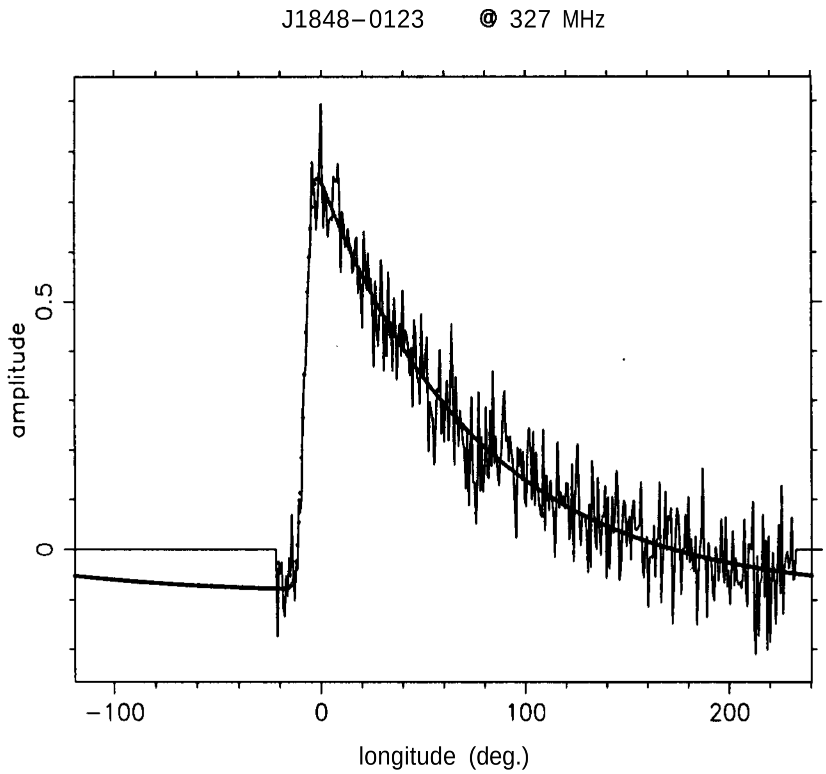

Figure 5.2: The observed pulse profile of PSR B1848-0123 at 327 MHz. The solid line gives the best fit model for the pulse, with the scattering delay of 141 ± 19 msec.

up to produce a single time series with a time resolution of 102.4μsec. These time series are averaged, synchronous with the apparent pulse period, over blocks of every 2^{15} sample points separately to obtain a set of sub-average profiles using a specified number of bins across the pulse period. The mean total power (in some arbitrary units) is computed and subtracted from the average profile for each block. The subtracted means of all the blocks are stored separately and were used for flux calibration (for more details of this processor see McConnell et al. 1996).

5.3.2 Sample selection

We selected a set of candidates for which the expected pulse broadening[1] due to scattering is greater than 40% of the effective pulse width. The pulse broadening estimates include the dispersion smearing over the spectral resolution used, the broadening introduced by the finite time resolution of the receiver and the intrinsic pulse width (taken from the pulsar catalogue of Taylor et al. 1993). In cases where the pulse widths at higher frequency were not available an intrinsic duty-cycle of 4% was assumed. With the above mentioned criteria a set of 27 candidates were selected for observations.

5.3.3 Analysis and results

The sub-average profiles for a given pulsar were further combined to produce an observed average pulse profile. The scatter broadening was estimated using a least,-square-fit to the observed profile as discussed below.

The observed pulse profile $y(t)$ is the convolution of intrinsic pulse shape $x(t)$ with: a) the impulse response characterising the scatter broadening in the ISM, $s(t)$. b) the dispersion measure across the narrow spectral channel, $d(t)$ and c) the instrumental impulse response, $i(t)$. That is,

$$y(t) \;=\; x(t) \otimes s(t) \otimes d(t) \otimes i(t) \tag{5.1}$$

where $\otimes$ denotes convolution. In a simplistic picture, the scattering is assumed to take place at a thin screen as discussed in section 1.10. The impulse response function characterising the interstellar scatter broadening can then be written as

$$s(t) \;=\; \exp(-t/\tau_{\rm sc}) \tag{5.2}$$

We assume an impulse function for $d(t)$ where the width of the function is the dispersion smearing across the finite width of the frequency channels given by equation 1.23. The

---

[1]The expected pulse broadening (τ_{sc}) was calculated using the Taylor & Cordes (1993) electron density model of the galaxy. The method is described in section 5.4.2 and we have used equation 5.11 to calculate the value of τ_{sc} at 1 GHz. The values were scaled to 327 MHz using a frequency dependence of $\nu^{-4.4}$ for τ_{sc}

instrumental response $i(t)$ is also assumed to be an impulse function with the width being the finite sampling time of the data. For a Kolmogorov power spectrum given by, $P_{\delta n_e}(q) = C_n^2 q^{-11/3}$, where q is the wave number, the value of τ_{sc} depends on the frequency ν and the dispersion measure (DM) as $\nu^{-4.4}$ and $DM^{2.2}$ respectively (see section 1.10).

The intrinsic pulse shape was assumed to be a gaussian with half-power width w_0. The template of the scatter broadened pulse profile can be produced by convolving the different responses with a gaussian as given by equation 5.1. The dispersion smearing (due to the finite width of the frequency channels) is considered corresponding to a channel width of 10 kHz. However in most cases the smearing can be ignored as a dispersion measure of 425 pc cm^{-3} produces a smearing of only about a millisecond.

Many different combinations of τ_{sc} and w_0 were tried in a suitable grid search to look for the best match between the observed average pulse and the predicted pulse template. In some cases, where it is suspected that the intrinsic pulse profile may have two components, we have assumed an intrinsic pulse profile consisting of two gaussians with an assumed separation while solving for the ratio of their heights and a common value for their widths. The best fit was produced by minimising the normalised χ^2 value defined by,

$$\chi^2 = \frac{1}{N_{\mathrm{dof}}\sigma_n^2}\sum_{i=1}^{N}[y_i^o(t) - y_i^m(t)]^2 \tag{5.3}$$

where, σ_n is the root mean square noise value of the off-pulse, y^o is the observed pulse profile and y^m is the model pulse profile. The y^m profile is similar to $y(t)$ except for an amplitude scale factor and a constant offset in phase and baseline that minimises χ^2. N is the number of points used, and N_{dof} is the number of degrees of freedom.

The observed profiles and fits for all 27 pulsars are shown in figure 5.8. In figure 5.2 we show an enlarged view of the observed profile and the model fit for PSR J1848-0123. The best fit scatter broadening for this pulsar is 141.2 milliseconds.

The results of the analysis are listed in table 5.1. The table lists against the name of each pulsar, its dispersion measure, the observed average flux density at 327 MHz, the estimated scatter broadening (τ_{sc}) and its error bar, an estimate of the intrinsic width (w_i) and its error bar, the correlated error on ($\tau_{sc} + w_i$), the value of the minimum

χ^2 obtained, the number of degrees of freedom, and the expected scatter broadening according to the free electron density distribution model of Taylor & Cordes (1993). The error bars correspond to 99.99% confidence level.

5.3.4 Flux calibration

As mentioned in section 5.2, the total-power estimate for each subaveraged profile were recorded. For simplicity, a mean of these estimates were computed for each observation, assuming that the system parameters were constant within the 30 min integration time. This mean is the sum of the contribution from the system temperature C_s and the pulsar C_p, i.e. mean=$(C_\mathrm{s} + C_\mathrm{p})$. The average pulse contribution was estimated from the average profile in order to estimate the contribution of C_s which is proportional to the system temperature alone. The system temperature was estimated by assuming the receiver temperature to be 110 K (Selvanayagam et al. 1993), and computing the sky background temperature at 327 MHz. This has been obtained by extrapolating the sky background temperature given in the 408 MHz survey of Haslam et al. (1982) (using a frequency dependence of $\nu^{-2.5}$). The sensitivity of the ORT was estimated to be about (2.5 K/Jy) $\cos\delta$, using a large number of continuum calibration sources with δ being the declination of the source. This gave us the provision to calculate the average flux of the observed pulsars at, 327 MHz. The flux values thus calculated are listed in table 5.1.

However, it should be pointed out that our typical observation time for each pulsar was only one session of about 30 min., which may not be enough to average out the variations of pulsar flux due to various systematic effects. This is particularly so if the pulsar signal is highly linearly polarised and considering that ORT responds to only single linear polarisation and the observing bandwidth was only 10 MHz. Moreover, the explicit declination dependence of the gain variation of the ORT system is not well calibrated, especially at high declinations.

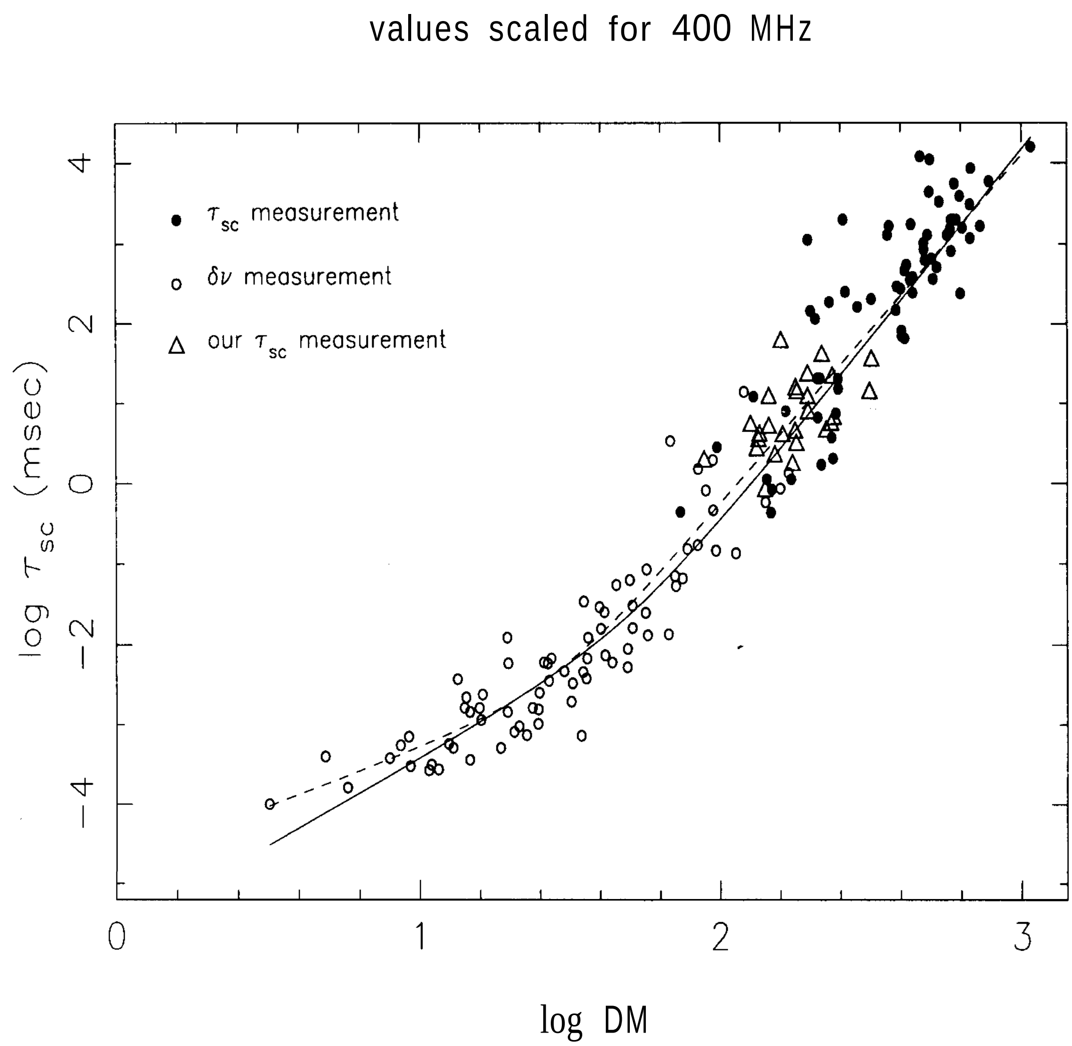

Figure 5.3: Observed scatter broadening as a function of dispersion measure, for 167 pulsars. Triangles represent our scattering delay measurements, Open circles represent the scattering delay calculated from the decorrelation band-width measurement with the relation $2\pi\nu\tau_{sc} = 1$, filled circles represent the directly measured scatter broadening. The values corresponding to open and filled circles are taken from the Princeton pulsar catalogue of Taylor et al. (1993). The best fit models of the form, τ_{sc} = A DM" (1+ B DM^{γ}), with value of $a = 2.2$ and $\alpha = 1.47$ are shown as continuous and broken lines (see text for more details).

5.3.5 Discussion and Conclusion

Out of our 27 measurements only one (PSR J1848–0123) had been measured earlier, for which the measured scatter broadening at 430 MHz is 42 msec (Cordes et al. 1955). For an assumed dependence of $\lambda^{4.4}$ corresponding to the Kolmogorov spectrum for irregularities, the expected scattering delay is about 140 msec. As table 5.1 shows, the measured value is 141 ± 19 msec, quite consistent with the measurement at the higher frequency. It may be worth mentioning here that for this pulsar the scattering delay predicted by the electron density model of Taylor & Cordes (1993) however is only 17 msec at 327 MHz.

As Figure 5.2 shows, the profile has a distinct sharp rise, and then an exponential fall-off, indicating that the scatter broadening is dominated by a single scattering screen along the line of sight. The measured distance of 3.8 kpc to this pulsar and its direction ($l = 31^{\circ}.339$, b $= 0^{\circ}.039$) indicate that it lies behind the Sagittarius arm which may probably explain the enhanced scattering.

One of the conventional methods of examining the scattering properties along various lines of sight is to plot the dispersion measure versus the measured scatter broadening. What is plotted in figure 5.3 is τ_{sc} (at 400 MHz) versus DM for 167 pulsars, which includes the 26 new measurements. The open circles indicate the scatter broadening estimates based on the decorrelation bandwidth measurements; the open triangles represent our scatter broadening measurements with the ORT, and the filled circles indicate earlier direct measurements of scatter broadening. The τ_{sc} values were scaled to 400 MHz assuming a frequency dependence of $\nu^{-4.4}$. A line-fit for the direct τ_{sc} measurements (filled circles and triangles) show a slope of 4.3 ± 0.4, and the corresponding slope for τ_{sc} measurements estimated through the decorrelation bandwidth measurements is 2.7 ± 0.3. It is interesting that similar results are obtained when the DM dependence is considered in two separate DM ranges. The decorrelation bandwidth measurements available for pulsars with $DM > 100$ pc cm^{-3} seem to suggest that the steepening of the τ_{sc} dependence with DM is real and is not related to the fact that, the dependence appears to change with the kind of measurement used.

Sutton (1971) and Rickett (1977) have noted that for $DM \lesssim 20$ pc cm^{-3} the measured scattering delay increases roughly as DM^2, but for $20 \lesssim DM \lesssim 400$ pc cm^{-3} the relationship steepens considerably, to give a slope of about 4. This is essentially what is seen from figure 5.3. For DM less than about 100 pc cm^{-3}, $\tau_{\rm sc}$ (derived mainly from the decorrelation bandwidth measurements) values fit best for power law index of 2.7 ± 0.3. This is not significantly different from the expected slope of 2.2 for a Kolmogorov spectrum. However, for DM greater than about 100 pc cm^{-3} the observed slope is significantly higher (4.3 ± 0.4) than 2.2.

At this point, it may be worth recalling the assumptions which have gone in expecting the dependence of scatter broadening on various physical parameters. If one assumed that (i) $\delta n_{\rm e} \propto n_e$, (ii) DM $\propto$ distance, (iii) the scattering along the line of sight can be assumed to be confined to a thin screen half way down the line of sight, and (iv) the spectrum of wave numbers follows a power law of index $11/3$ (Kolmogorov spectrum), then we get a relation (Romani et al. 1986),

$$\tau_{\rm sc} \propto C_{-4}^{1.2}\ \lambda^{4.4}\ DM^{2.2} \tag{5.4}$$

where, $C_{-4} = 10^4 C_{\rm n}^2$ and λ is the wavelength of observation. For $DM > 100$ pc cm^{-3} it is clear that some of the assumptions become invalid. The existence of isolated regions of enhanced scattering along sight lines to many pulsars and the consequent probable failure of the assumption that the scatterer is half-way down the sight line, can very well explain the large deviation of the observed scattering from the mean trends, in both of the DM ranges. However, a very systematic change in the DM dependence needs to be understood differently. Rickett (1977) argued that the steep dependence of $\tau_{\rm sc}$ on DM is the manifestation of large scale variation of $C_{\rm n}^2$ in the Galaxy. However, Hall (1980) argued that it is due to the large scale variation of the mean electron density. Cordes et al. (1985) analysed various possibilities, and came to a conclusion which agrees with that of Rickett (1977).

One should keep in mind that at higher DM, one is essentially looking in the central regions of the Galaxy. Instead of the assumption that the density fluctuation $\delta n_e \propto n_e$, it is more appropriate to assume a galactocentric radius (R) dependence of $\delta n_e \propto n_e.{\rm f}({\rm R})$, where f (R) is a suitable function of R. In order to explain the

Name	**DM** (pc/cc)	S_{327} (mJy)	$\tau_{\rm sc}$ (ms)	$\Delta\tau_{\rm sc}$ (ms)	w_i (ms)	Δw_i (ms)	$\Delta(\tau_{\rm sc}+w_i)$ (ms)	χ^2	$N_{\rm dof}$	$\tau_{\rm c}$
J0738-4042	160.8	105	76	3	20	3	3	1.2	485	0.3
J1209-5556	174.0	3	4	2	2	2	2	1.0	55	10
J1556-4258	145	20	12	2	5	1	1	1.0	167	6
J1604-4909	140.8	16	2	2	5	3	1	1.3	55	11
J1613-4714	161.3	16	9	3	7	3	2	1.2	117	15
J1615-3936	152	7	5	5	8	5	3	0.9	75	6
J1651-5222	179.1	15	7	2	8	2	2	1.3	101	13
J1705-3422	145	18	29	7	16	6	5	1.1	488	11
J1722-3207	126.035	126	13	1	6	1	1	1.5	125	11
J1732-4128	195	12	28	9	13	11	8	1.0	197	18
J1745-3040	88.4	79	5	1	4	1	1	1.3	121	5
J1750-3506	195	11	54	52	99	45	30	1.0	113	20
J1757-2421	178.0	18	36	20	10	25	14	1.0	113	28
J1759-2205	177.3	50	10	2	4	2	1	1.2	90	27
J1807-2715	313.3	26	32	8	16	5	5	1.1	147	9
J1823-0154	135	7	10	3	5	4	2	1.1	70	9
J1829-1751	217.8	74	96	18	33	6	6	1.1	502	32
J1833-0338	235.8	132	51	2	19	2	2	1.2	207	40
J1835-1106	132	33	6	2	7	2	2	1.0	137	13
J1836-1008	318	32	83	61	112	63	33	1.3	98	152
J1848-0123	159.1	121	141	19	14	7	6	1.0	487	17
J1848-1414	134	7	8	10	12	12	5	1.1	37	8
J1902+0556	179.7	29	33	16	21	12	11	0.9	157	15
J1903-0632	195.7	45	18	1	9	2	1	1.2	317	12
J1904+0004	234	12	13	6	18	6	4	1.2	493	36
J1905-0056	225	18	11	3	11	3	2	1.0	107	26
J2013+3845	238.6	27	15	6	24	7	4	1.1	493	15

Table 5.1: Results. The table lists the pulsar Jname, its dispersion measure, flux at 327 MHz, best fit scatter broadening at 327 MHz and its error corresponding to 99.99% confidence level, the best fit intrinsic width and its error corresponding to 99.99% confidence level, the correlated error on (τ_{sc} + w,), the normalised χ^2, the degrees of freedom, and the expected scatter broadening according to the electron density model of Taylor & Cordes (1993).

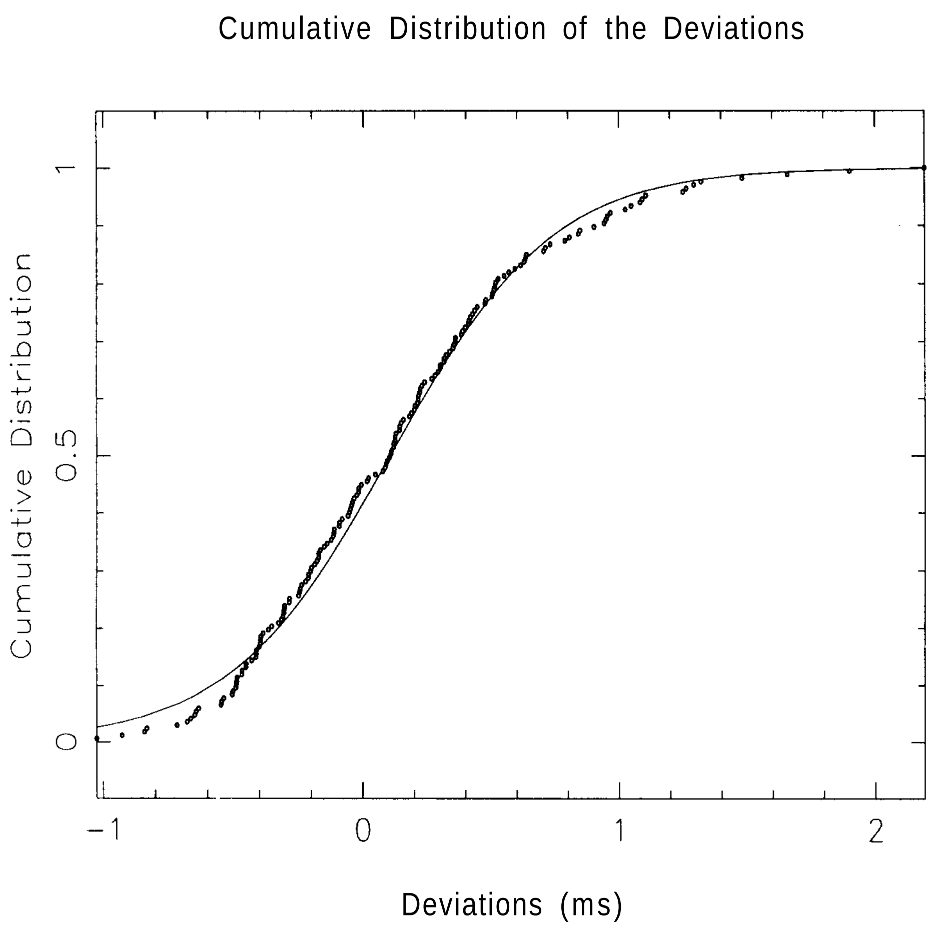

Figure 5.4: The cumulative distribution of the observed deviation from the mean dependence as given by equation 5.7 is plotted as function of deviations given by the dotted points. The solid line corresponds to 'he curve given by equation (1.26) corresponding θ=0.106 and ϕ=0.313.

observed enhanced scattering for higher DM's, such a dependence in some sense is already incorporated in the electron density distribution model of Taylor and Cordes (1993). Our new measurements sample a useful volume of the inner galaxy and hence should help in the refinement of this model. As can be seen from table 5.1, in more than half of the directions the broadening observed differs by significant factors, from that predicted by the model. These deviations are unlikely to be due to lack of local enhancements (other than the Gum region) being incorporated in the model., This is because most of our pulsars have DM $>$ 100 pc cm^{-3} and hence somewhat too distant to see appreciable contribution from the local HII regions.

For the purpose of many statistical studies of the pulsar population, it is useful if the mean dependence of τ_{sc} on DM can be modeled in a simple manner, spanning the entire range of DM's observed. Although similar attempts have been made earlier, the sample available then was much smaller in size (see for example; Bhattacharya et al 1992). We have considered a functional form given by,

$$\tau_{sc} = A\ \mathrm{DM}^{\alpha}\ (1 + B\ \mathrm{DM}^{\gamma})\ \lambda^{4.4} \tag{5.5}$$

and sought values for (A, α, B, γ), which fit the observed mean dependence of $\log \tau_{sc}$ on $\log(DM)$ as shown in figure 5.3. The best fit model of the above form is found to be,

$$\begin{aligned} \tau_{sc}(\mathrm{ms}) &= 4.2 \times 10^{-5}\ DM^{1.6} \\ & \quad \times (1 + 3.1 \times 10^{-5}\ DM^{3})\ \lambda^{4.4} \end{aligned} \tag{5.6}$$

and is shown in figure 2 (as dashed curve). Here, λ is substituted in metres. We have also attempted similar modelling with the values of α fixed to 2.2 (corresponding to the dependence expected from Kolmogorov spectrum for electron density fluctuation). This gives us a relation,

$$\begin{aligned} \tau_{sc}(\mathrm{ms}) &= 8.4 \times 10^{-6}\ DM^{2.2} \\ & \quad \times (1 + 8.3 \times 10^{-5}\ DM^{2.5})\ \lambda^{4.4} \end{aligned} \tag{5.7}$$

where the term $(1 + B\ DM^{\gamma})$ should provide a useful description of the apparent mean dependence on the the turbulence level on DM.

We also model the distribution of the observed deviation from this mean dependence (ref. eq. 5.7). Bhattacharya et al. (1992), for a similar modelling, had used a functional form given by,

$$P(\delta \log \tau_{sc}) = \left[1 + \exp\left(\frac{\theta - 6 \log \tau_{sc}}{\phi}\right)\right]^{-1} \tag{5.8}$$

where $p(\delta \log \tau_{sc})$ is the cumulative distribution of the deviations and 8 and ϕ are constants (refer Fig. 5.4). While it is possible to find a better functional form, we have used the above functional form as it is found to provide an adequate description in the present case as well. However, we obtain the values of 8 and ϕ to be 0.106 and 0.313 respectively, compared with the values 0.04 and 0.342 as obtained by Bhattacharya et al. (1992). The positive deviations are probably due to the existence of regions of enhanced turbulence while the negative deviations may be attributed to the possibility that the effective scatterer location may be much closer to the pulsar or the observer rather than being midway between them.

5.4 Scattering of pulsar signals due to the Gum nebula

The gum nebula (first observed by Gum 1952, 1956) is the most remarkable galactic nebula not only because of its proximity but also because it has the most extended *Ha* emission. The nebula extends for about 40" in angular size centered around galactic longitude $l \sim 255$" and galactic latitude b $\sim -2°$. The distance to the nebula is found to be approximately $\sim$ 400pc. Since the discovery of the gum nebula its origin has been an extremely controversial topic which has not been resolved till now. There are several theories for the nature of the gum nebula and we briefly mention a few here. For a detailed review of the Gum Nebula see Bruhweiler et al. (1983).

The Gum Nebula appears extremely diffuse and faint in *Ha* thus making it extremely difficult to estimate its size. One of the earliest measurements gave its size to be as large as 75° x 45" (Brandt et al. 1971). Refined estimates of the size of the nebula using wide field Hα imaging is given by Sivan (1974), which restricts the size to $\sim 36°$. Based on a spectroscopic study of ionized gas, Reynolds (1976 a,b) proposed that the Nebula is an one million year old expanding gas shell, originally produced by a supernova explosion, which is now being heated and ionized by ζ Puppis and γ^2 Velorum.

According to Weaver et al. (1977), the stellar wind from ζ Puppis could be strong enough to produce the observed Nebula which is a shell. The shell is formed by the interaction of the stellar winds from ζ Puppis and γ^2 Velorum with the ambient interstellar medium. They also predict soft X-rays from the hot interior, which is at a temperature of about 10^6K. Wallerstein et al. (1980) from a study of the interstellar gas towards stars in the direction of the nebula came to the conclusion that the nebula is consistent with a model of the Gum Nebula as an HII region ionized by OB stars and stirred up by multiple stellar winds. Chanot & Sivan (1983), on the basis of 60"-field *Ha* photographs suggested that the Gum Nebula is composed of two regions, one which is a circular main body with a typical ring-like appearance of diameter of 36°, and the other consist of faint diffuse and filamentary extensions which merge with the faint H a background. This idea supports the model of Reynolds (1976 a) for an expanding *Ha* shell ionized by UV flux of ζ Puppis and γ^2 Velorum. The origin of the shell structure is however uncertain.

From a detailed study of the Gum Nebula Sahu (1992) came to the conclusion that the nebula is a shell like structure surrounding the Vela R2 association which is at a distance of about 800 pc while the shell like structure near the Vela OB2 association known as the IRAS Vela shell is at a distance of about 450 Kpc. This hypothesis crucially depended on the distance to ζ Puppis as this star is believed to be the primary source of ionization of the Gum Nebula, which Sahu (1992) found to be $\sim$ 800 pc. However the Hipparcos distance estimates to ζ Puppis rules out the above scenario. Rajagopal (1999) showed from the kinematics of the IRAS Vela shell that the Gum Nebula is either inside or overlapping with the shell.

The various possible alternative scenarios as discussed above has left several open ends in our understanding of the Gum Nebula. The electron density estimates inside the Gum Nebula as shown by Reynolds (1976a), and Wallerstein et al. (1980), show large variations –from 0.1 to 100 cm^{-3}. The complicated structure of the nehula is also evident from the Hα images available (e.g. Chanot & Sivan, 1983).

In a study to obtain pulsar distances arid the electron density model of the galaxy Taylor & Cordes (1993) used the shapes and locations of various HII regions derived frorn existing optical and radio observations. In their model the Gum Nebula (because of its proximity) has been given special attention apart from tlie already existing HII regions which closely follow the spiral arms of the galaxy. However, as also suggested by Taylor arid Cordes, inadequate knowledge about the variations of the electron density and its fluctuations across the region makes it difficult to allow a meaningful model for the parameters of the Gum Nebula. We liave done a systematic survey across the Gum Nebula to measure the scatter broadening of pulsars due to the electron density fluctuations which should help in a better understanding of this extremelv complex region.

5.4.1 Source Selection and Observation

40 pulsars in the direction of the Gum Nebula, lying between galactic longitude 250° to 290° and galactic latitude −20° to 20°, were observed using the ORT (luring March 1997. In tlie specified region there are 48 pulsars found in pulsar catalouge (Taylor et al. 1993), however our sample is restricted to 40 pulsars as me choose pulsars having average flux above 5 mJy at 400 MHz. The DM of the observed pulsars range from 30 pc cm^{-3} to 306 pc cm^{-3}. Our sample includes pulsars for which scattering measurements exist at other frequencies.

To carry out these observations we liave used a pulsar receiver that was mainly built for pulsar searches (Ramkumar et al. 1994). The schematic diagram of the pulsar receiver is shown in figure 5.5. The pulsar receiver consists of a 4-bit sampler (Analog-to-digital converter), which samples the incoming signal voltage of bandwidth 8 MHz. The output of this is fed to an FFT engine. The FFT produces 256-point complex spectra which are converted to power spectra using look-up tables. The resultant power spectra are pre-integrated over successive spans of $\sim$ 0.5 msec, which is tlie final time resolution in recorded data. A block integration is done over a number of pre-integrated

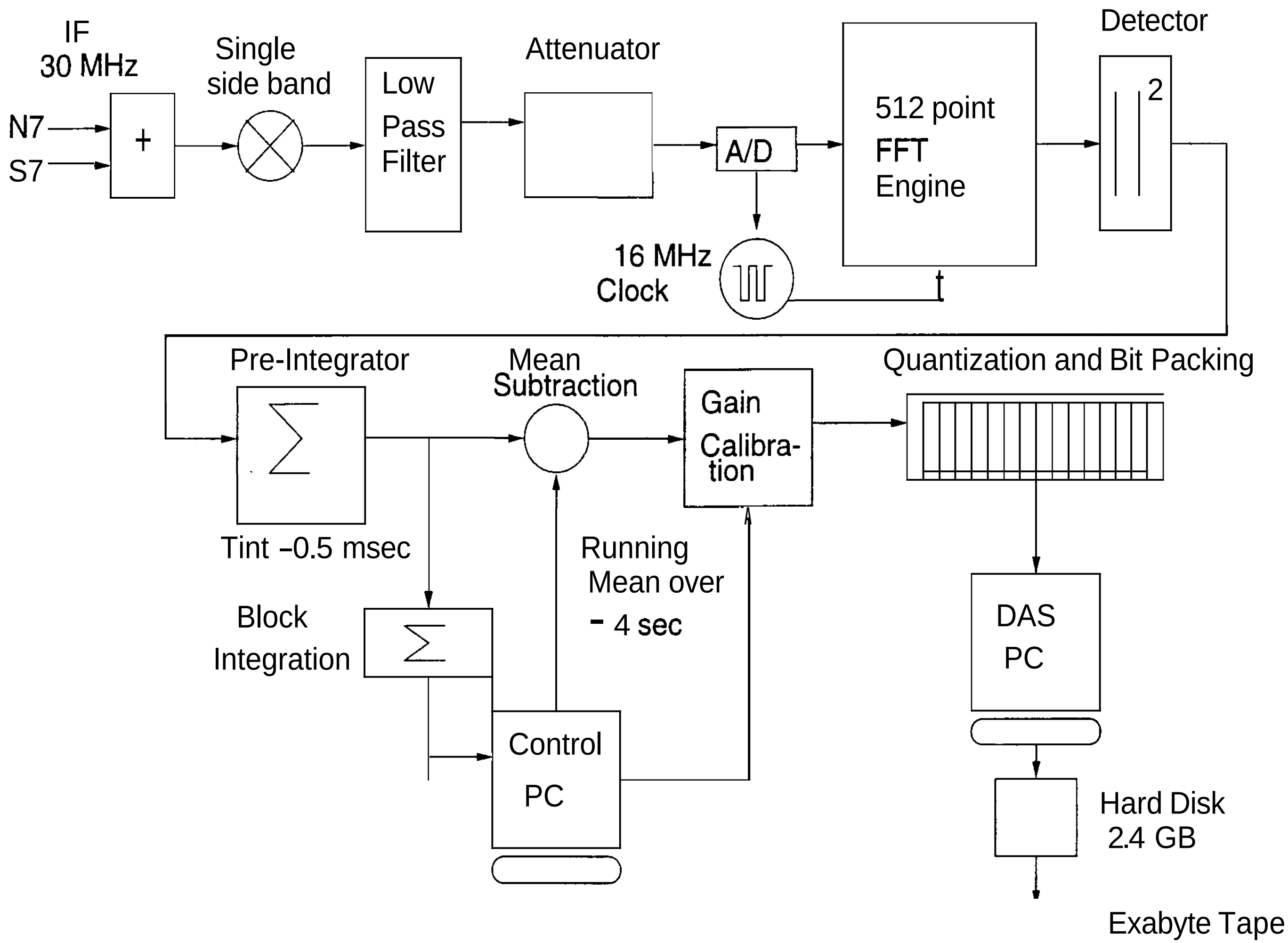

Figure 5.5: Schematic diagram showing the Pulsar receiver system used in Ooty Radi telescope. For further details of the receiver see Ramkumar et al. (1994).

samples for calculation of the running mean for each of the 256 frequency channels. The running mean is finally subtracted from the pre-integrated data to remove the effects of receiver gain variations. The mean subtracted pre-integrated data is then represented as a one-hit signal by recording the sign bit and stored on magnetic tape. We observed each pulsar for 20 min, and used offline dedispersion and folding to obtain the integrated pulse profiles.

Out of the 40 pulsars observed only 21 were above our detection limit. Using the technique described in section 5.3.3 the folded dedispersed pulse profiles were analysed to yield measurements of scatter broadening. The results are given in Table 5.2, and the observed profiles and the model fits are displayed in figure 5.9. In Table 5.2, the pulsars PSR 50742-2822, PSR 50745-5351 and PSR J0835-4510 were not observed by us, but we have used scattering measurements reported in the literature (Roberts & Ables 1982, Alukar et al. 1986). In cases where the reported scatter broadening was at a frequency different from 327 MHz, we have used the $\nu^{-4.4}$ scaling to obtain values appropriate to 327 MHz. PSR's J0809-4753, J0837-4145 and J0840-5332 in Table 5.2 have had their scatter broadening reported earlier at frequencies other than 327 MHz, but we have reobserved them and the scatter broadening as listed in the table come from our measurements. The spatial distribution of the pulsars across the Gum Nebula is shown in figure 5.6.

5.4.2 Discussion

In figure 5.7 we have plotted the new values τ_{sc} as obtained in and around the Gum Nebula as a function of DM. The deviations from the Kolmogorov law (dark line in the figure) seems to be more than is seen in figure 5.3. As already discussed, these deviations are probably due to either enhanced turbulence in the medium or due to the fact that the scattering material is not located midway between the pulsar and the observer. In figure 5.7, PSR J1924-5814 seems to have a large deviation compared to the rest of the points. However the error in the estimate of τ_{sc} for this pulsar is more than 100% (refer table 5.2) due to poor signal to noise ratio of the integrated pulse profile. It is interesting to note that the distribution of pulsars in the Gum Nebula

PSR Jname	DM pc/cc	τ_{sc} msec	w_i msec	$\Delta(\tau_{sc} + w_i)$ msec	N_{dof}	χ^2	F	Distance
J0738-4042	160.8	76 ± 3					6.3	4.5
J0742-2822[1]	73.7	1					0.8	0.65
JO745-5351'	122.3	60					7.0	4.11
J0809-4753[2]	228.3	79 ± 18	9 ±10	8	697	1.03	5.9	>12.65
J0820-4114	113.4	30 ± 11	42 ±14	9	216	1.23	6.6	0.64
J0835-4510[1]	68.2	8					6.3	0.50
J0837-4135[2]	147.6	1 ± 1	9 ±3	2	597	3	0.0	1.89
J0840-5332[2]	156.5	57 ± 11	13 ±10	10	218	1.1	5.3	4.25
J0846-3533	91.1	4 ± 5	44 f 6	5	135	2.1	1.7	0.58
J0855-3331	87.7	1 ± 3	24 ±1.5	1	595	1.3	0.0	0.57
J0904-4246	189	8 ± 4	21 f 4	3	397	0.99	0.8	4.6
J0905-5127	189	4 ± 7	11 f 8	5	218	0.88	0.5	5.54
J0907-5157	104	1 ± 13	32 ±10	10	228	0.9	0.15	0.88
J0924-5302	152.9	1 ± 1	6 ±0.8	1	195	1.1	0.15	4.02
J0924-5814	60.0	55 ± 65	1 ±50	45	238	1.0		
J0934-5249	99.4	7 ± 13	21 ±10	5	197	1.1	1.3	1.66
J0942-5552	180.2	5 ± 1.5	7 f 2	2	237	1.1	0.3	5.28
J0952-3839	167	2 ± 12	48 f 10	8	227	0.91	0.25	>8.46
J0955-5304	156.9	3 ± 1	5 f 1	1	122	1.2	0.67	4.25
J1001-5507	130.6	15 ± 2	13 ±2	2	197	1.1	10.7	3.44
J1003-4747	98.1	0 ± 4	9 f 4	3	197	1.2		
J1017-5621	439.1	16 ± 36	8 ±25	25	228	0.97		
J1042-5521	306	7 ± 10	29 ±10	10	238	1.1		
J1046-5813	240.2	43 ± 50	2 ±50	50	238	1.03		
J1059-5742	107.9	2 ± 3	20 ±7	5	237	1.2		

Tahle 5.2: Values of the τ_{sc} obtained for pulsars in the direction of the Gum Nebula. Pulsar names bearing superscript 1 are those for which τ_{sc} values are obtained from earlier measurements: these were not observed by us. Pulsars with superscript 2 are those for which τ_{sc} earlier measured values are available, but have also been reobserved by us. The expected results are in good agreement with our measurements. PSR J0738-4042 was a part of the sample during the earlier part of our survey and the τ_{sc} values is taken from table 5.1. Column 1, 2, 3 and 4 lists: the pulsar Jname, DM, the best fit scatter broadening τ_{sc} and its error corresponding to 99.99% confidence level, the intrinsic pulse width w_i and its error corresponding to 99.99% confidence level. Column 5, 6 and 7 lists the correlated error on $(\tau_{sc} + w_i)$, the normalised χ^2 and the number of degrees of freedom respectively. In column 8 and 9 the fluctuation parameter F and the distance obtained to the pulsar (D) is given (see text for details).

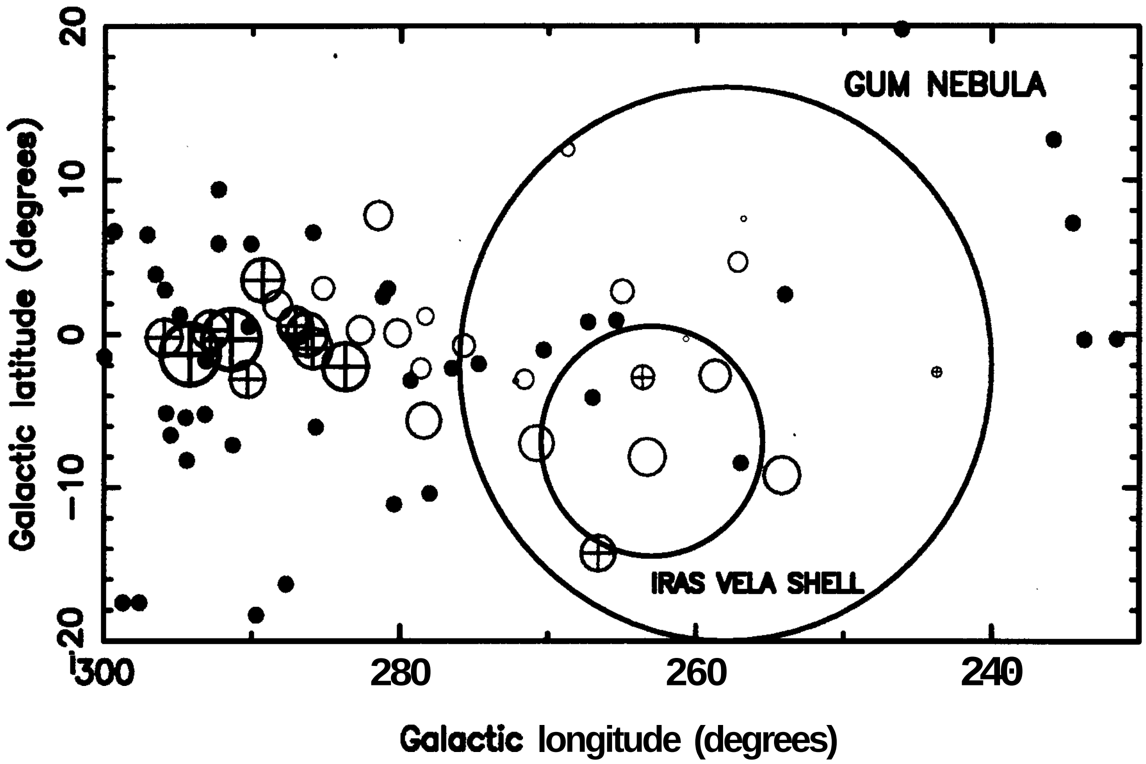

Figure 5.6: Observed scatter broadening (τ_{sc}) of pulsars at 327 MHz plotted as a function of galactic longitude (1) and galactic latitude (b) as seen in the sky around the Gum Nebula region. The green circles with crosses correspond to pulsars for which earlier scatter broadening measurements are available. The magenta coloured open circles are pulsars for which scatter broadening measurements are available at other frequencies and we have reobserved them at 327 MHz. The red open circles are the pulsars observed using ORT. The size of the circles is proportional to $log(\tau_{sc})$, where τ_{sc} is in milliseconds. The blue dots are pulsars for which τ_{sc} measurements are not available. In the above plot, all known pulsars in the region as available in the pulsar catalogue (Taylor et al 1993) are plotted. The big circle labeled as the Gum Nebula corresponds to a radius of 18" with the morphological center as $l = 258°$ and b $= -2$" and the smaller circle which is labeled as the IRAS vela shell has a radius of $\sim$ 7.5" and corresponds to $l = 263°$ and b $= -7$": these values were adopted from Sahu (1992). Note that our sample consists of pulsars which lie outside the 'main body' of the Gum Nebula suggested by Chanot & Sivan (1983). We include these pulsars as the exact size of the Gum Nebula is not known and it is possible that the faint diffuse and filamentary

values scaled for 400 MHz

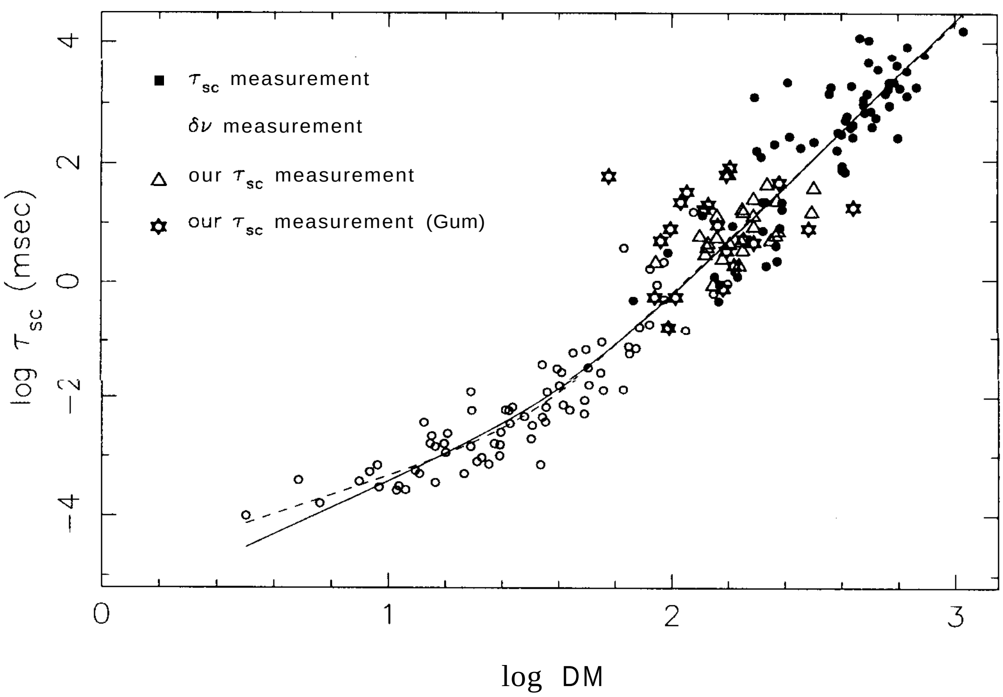

Figure 5.7: This figure is similar to figure 5.3, except here the new measurements obtained for pulsars in the direction of the Gum Nebula is added, which are the points marked as stars in the plot.

region shown in figure 5.6 is skewed to one side (mostly lying between longitude range of 255° to 275°) of the nebula marked by the large circle in the figure. Pulsars with high τ_{sc} appear to lie behind the IRAS vela shell as marked by the small circle in the figure.

The Gum Nebula has been invoked explicitly in models estimating pulsar distances and free electron density distribution of the galaxy (e.g. Lyne & Manchester 1985, Bhattacharya et al 1992, Taylor & Cordes 1993). The model of Taylor & Cordes (1993) is a hit more detailed than the others. The necessity for invoking the Gum Nebula arises because of the closeness of the nebula which becomes important while evaluating effects of the interstellar medium near $l \sim 260°$. They have assumed the Gum Nebula to be centered around $l = 260°$, b = 0° with an angular diameter of $\sim 40°$ and the nebula is placed at a distance of d = 0.5 kpc. They assumed a electron density of $n_g = 0.25 \mathrm{cm}^{-3}$ at the center of the nebula which is held constant over a distance to

130 pc, and falls off thereafter as a one-sided Gaussian with 50 pc lengthscale. Based on the scattering measures of only two pulsars available at that time in the direction of the Gum Nebula (out of which one was the Vela pulsar, PSR B0833-45, which shows enhanced scattering due to the vela supernova remnant, and the other PSR B0835-41 which has practically no scattering effects; see table 5.2) they concluded that only the small scale feature of the supernova remnant is responsible for scattering. Thus in their model the Gum Nebula simply enhances the DM's of pulsars but does not increase the scatter broadening. However, as is obvious from figure 5.6, the nebula does contribute to enhanced scattering of pulser signals. This issue was addressed by Deshpande & Ramachandran (1998), where they have explicitly shown that in order to explain the enhanced scattering observed for PSR J0738-4042, which is a pulsar in the Gum Nebula (refer table 5.2), one has to increase n_e, arid adopt values of fluctuation parameter almost equal to that of the spiral arm. We have used a similar method as suggested by Deshpande & Ramachandran (1998), and have obtained the distances and the fluctuation parameters for the pulsars behind the Gum Nebula under the framework of the Taylor & Cordes (1993) model, which we briefly describe below.

The electron density model as put, forward by Taylor & Cordes (1993) is semi-empirical in nature. There are four relevant observable quantities which carry information about the interstellar scattering of the radio signal. First is the DM of a pulsar which can be determined with great accuracy and is found as a part of the discovery process. The second is the angular broadening of the pulsar image, θ_s which is defined as the FWHM of the broadened image. The third is the scatter broadening of the pulsar, τ_{sc} and fourth is the characteristic bandwidth of diffractive scintillations, $\delta\nu_s$. θ_s, τ_{sc} and $\delta\nu_s$ are related to the scattering measure (SM) defined by,

$$SM = \int_0^d C_{\rm n}^2 ds \quad \text{kpc m}^{-20/3}, \tag{5.9}$$

where $C_{\rm n}^2$ is spectral coefficient for a truncated power-law spectrum of spatial fluctuations in the interstellar free-electron dcnsitv (see section 1.10). SM is related to θ_s and τ_{sc} by the following relations,

$$SM = \left(\frac{\theta_s}{71 \text{ mas}}\right)^{5/3} \nu_{\rm GHz}^{11/3} \quad \text{(galactic source)}, \tag{5.10}$$

$$\mathrm{S\,M} = 292 \left(\frac{\tau_{sc}}{d_{\mathrm{kpc}}}\right)^{5/6} \nu_{\mathrm{GHz}}^{11/3} \quad \text{(galactic source)}, \tag{5.11}$$

where mas stands for milliarcsecond and ν_{GHz} is tlie observing frequency in GHz and a Kolmogorov wave number spectrum is assumed for the fluctuations. d_{kpc} is the distance in kpc and τ_{sc} is in seconds. Scintillation bandwidth 611 is related to the temporal broadening by the relation $2\pi\delta\nu\tau_{sc} = 1$ (Sutton 1971). Note that these relations hold only in the strong scattering regime.

The high correlation between D M and SM of pulsars suggests that the electrons involved in dispersion are the same ones involved in scattering. Taylor and Cordes (1993) thus defines a dimensionless fluctuation parameter **F** as,

$$F = \frac{\zeta\epsilon^2}{\eta}\left(\frac{l}{1\ \mathrm{pc}}\right)^{-2/3}, \tag{5.12}$$

where ζ is the normalized variance of large scale electron density fluctuations, ϵ^2 the small–scale density variations, η is the volume filling factor for ionized regions, and l is the large scale limit for an assumed Kolmogorov power law of electron density. SM is related to **F** by the square of the volume averaged n,, and since different components along a line-of-sight are characterized by wildly varying SM, the expected differential SM is given by,

$$dSM = [3(2\pi)^{1/3}]^{-1} C_u F n_e^2 ds, \tag{5.13}$$

where tlie scale factor $C_u = 10.2\mathrm{m}^{-20/3}\mathrm{cm}^6$ gives SM in units of kpc $\mathrm{m}^{-20/3}$. As SM is cumulative, integrating the above equation along a line-of-sight over several discrete components can effectively give the total SM. However, for the Gum component in the Taylor and Cordes model **F** is zero.

Deshpande & Ramachandran (1998), showed that if the distance to a dominant discrete scatterer is known, then it is possible to use only the DM and the τ_{sc} measurements to find **F** and distances to pulsars lying behind tlie scattering region. They demonstrate that with the knowledge of four observable quantities namely, the angular broadening, temporal broadening, diffractive scintillation time-scale and the proper motion measurements it is possible to find the distance to a pulsar (also see Gwinn et al 1993). With the available data on the Vela pulsar and assuming the scatterer to be

400 pc away, they estimate the distance to the pulsar to be 500 pc. In the Taylor & Cordes model the Gum nebula is assumed to be at a distance of 500 pc with a radius of 180 pc and a central n_e of 0.25 cm^{-3}. By varying varying n_e and F and keeping the Vela pulsar at a fixed distance of 500 pc, Deshpande & Ramachandran (1998) found a value of $n_e = 0.32$cm^{-3} and F = 6.3, such that the observed DM (68.9 pc cm^{-3}) and τ_{sc} (8.25 msec at 327 MHz) are consistent. Applying this method to pulsar J0738-4042 they find similar values for F and n_e and in turn obtained a distance of $\sim$ 4.5 Kpc, instead of > 11 Kpc as given by the Taylor & Cordes model where $n_e = 0.25$cm^{-3} and F is zero. The reduction of the distance from 11 kpc to 4.5 kpc has far reaching implications, as the estimated velocity of the pulsar (from proper motion of about 72.5 mas yr^{-1}) which was originally thought to be > 3780 km s^{-1} (which was extremely high) was reduced to 1600 km s^{-1}.

Following the above findings it seems reasonable to assume that a major part of the Gum Nebula can be characterized by $n_e = 0.32$ cm^{-3} and a fluctuation parameter F = 6.3. In a simple exercise, for various lines-of-sight in the Gum Nebula we have applied the above technique to obtain F and distances to pulsars, keeping n_e fixed at 0.32. The values of F and distances (in kpc) obtained is given in table 5.2. We don't claim that these values are the absolute ones as various combinations of n_e and F can match the observed DM and τ_{sc}. However due to the calibration done using the Vela pulsar (Deshpande & Ramachandran, 1998), as mentioned above, these values might not be very unreasonable. It is interesting to note that most of the pulsars lying in the IRAS Vela shell seems to be consistent with a fluctuation parameter of $\sim$ 6.5, while the other regions in the Gum Nebula have an F of only —0.5. This, at least intuitively, indicates tliat the nebula and the IRAS Vela shell are two different entities with different fluctuation properties. Note that we have riot attempted any modelling of the region outside the Gum Nebula. The value of F for PSR J1001-5507 is 10.7 which we believe is too high to be associated with the nebula. For PSR J0924-5814, we get a value of 25 which is unreasonable, and this is due to the poor estimation of τ_{sc}. Thus we reject this pulsar in our analysis.

As an extension of the present study to a more detailed one, it would be interesting to establish the electron density variation of the Gum Nebula along the various lines-of-sight of these pulsars. Such estimates can be obtained from detailed Hα studies, which involves measuring emission measures in the line-of-sight to pulsars. The ratio of the emission measure and the DM can be used to estimate the electron densities. Though such estimates are available (Reynolds, 1976a), they are not sufficient for the entire set of lines-of-sight observed. Further, as we have estimated the scatter broadening of only a subset of pulsars in this region, there remains a significant fraction of pulsars for which such measurements are not available (as clearly seen in figure 5.6). With a more sensative instrument, it should be possible to enlarge the sample of scatter broadening measurements, shedding further light on the electron density fluctuations in this region.

Appendix

In this appendix we present the average pulse profiles of the sample of pulsars for which the scatter broadening were obtained at 327 MHz using the Ooty Radio Telescope. The data is plotted as a continuous line in each curve and the dotted line is the fit to the data given by the model equations 5.1.

The first 27 pulsars plotted in figure 5.8 are the observations listed in table 5.1 which were carried out using a special purpose pulsar processor (McConnell et al. 1996) The observational details are given in section 5.3.

The last 21 pulsars plotted in figure 5.9 are observations listed in table 5.2 for which the pulsar receiver (Ramkumar et al. 1994) was used. The details of the observations are given in section 5.4.

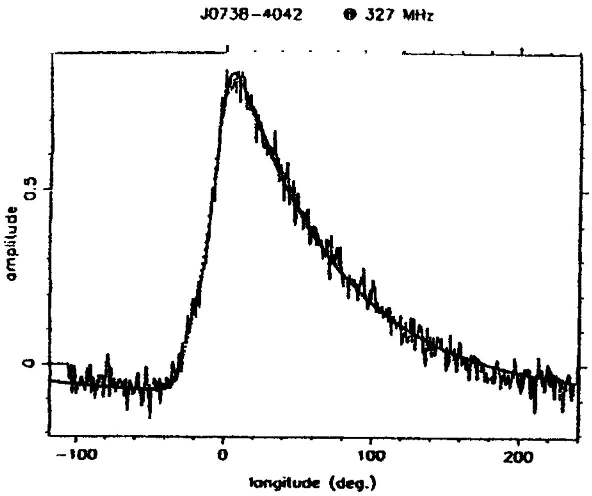
J0738-4042 ● 327 MHz
amplitude
0
0.5
-100
0
100
200
longitude (deg.)

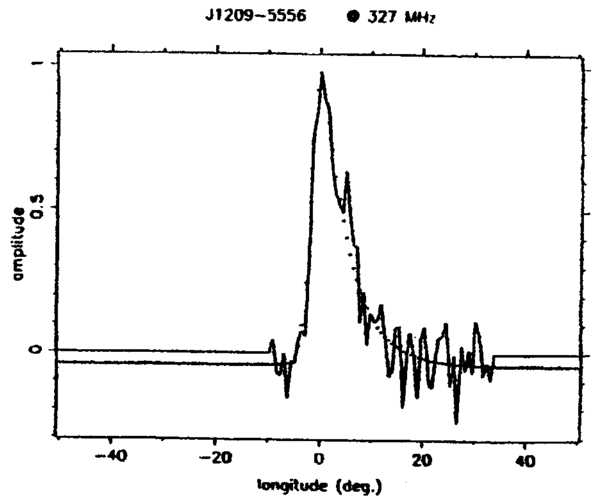
J1209-5556 ● 327 MHz
amplitude
0
0.5
1
-40
-20
0
20
40
longitude (deg.)

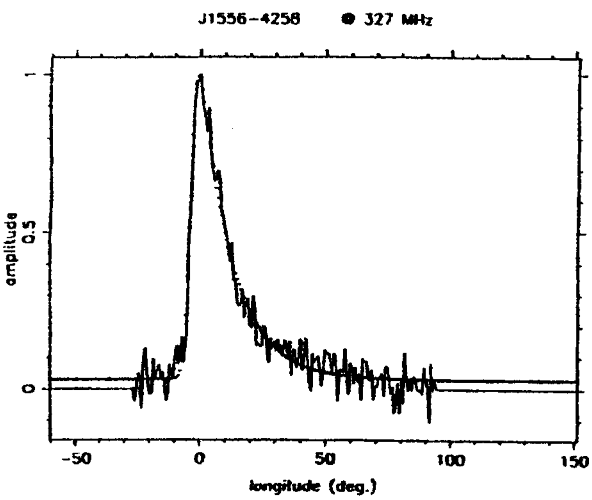
J1556-4258 ● 327 MHz
amplitude
0
0.5
1
-50
0
50
100
150
longitude (deg.)

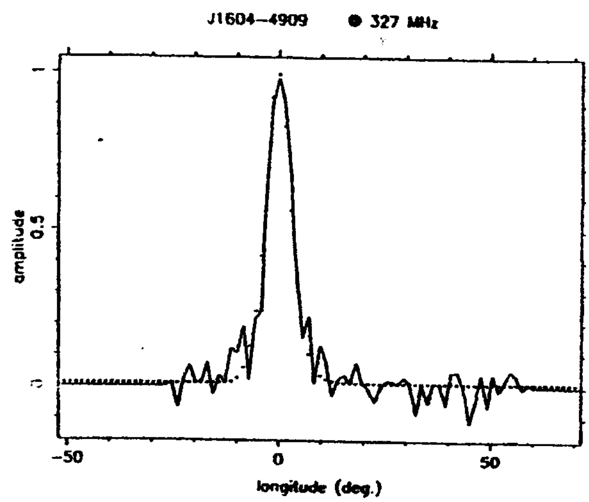
J1604-4909 ● 327 MHz
amplitude
0.5
1
-50
0
50
longitude (deg.)

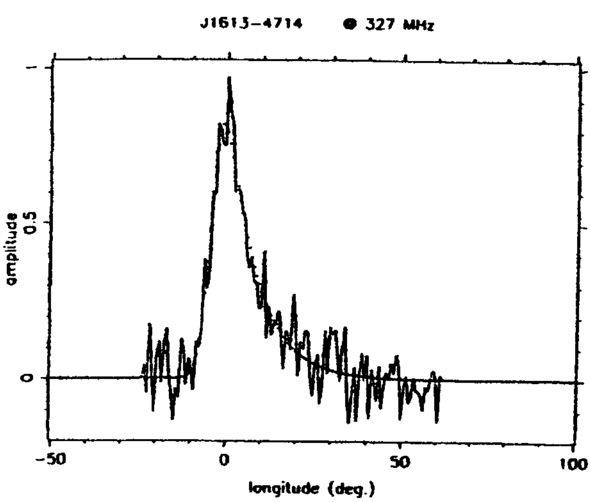
J1613-4714 ● 327 MHz
amplitude
0
0.5
1
-50
0
50
100
longitude (deg.)

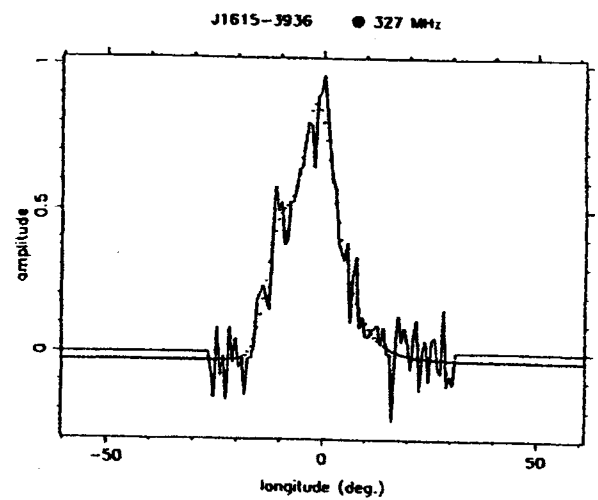
J1615-3936 ● 327 MHz
amplitude
0
0.5
1
-50
0
50
longitude (deg.)

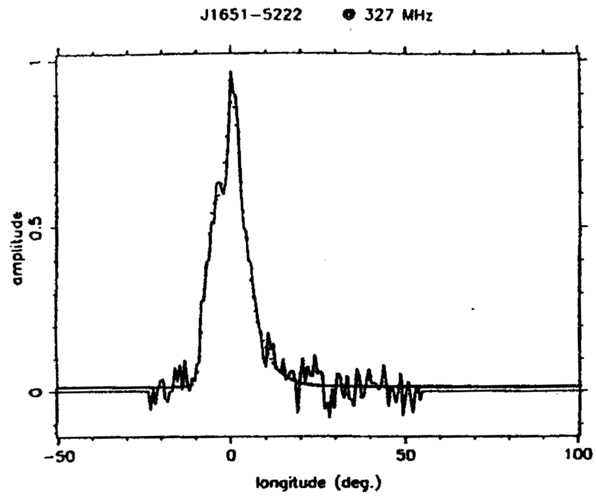
J1651−5222 ● 327 MHz
amplitude
0.5
0
−50
0
50
100
longitude (deg.)

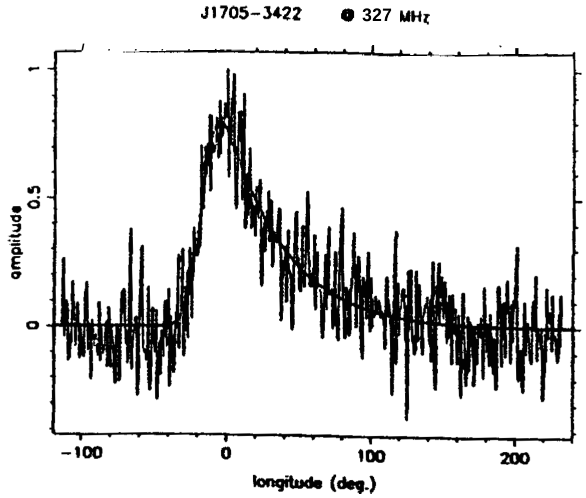
J1705−3422 ● 327 MHz
amplitude
1
0.5
0
−100
0
100
200
longitude (deg.)

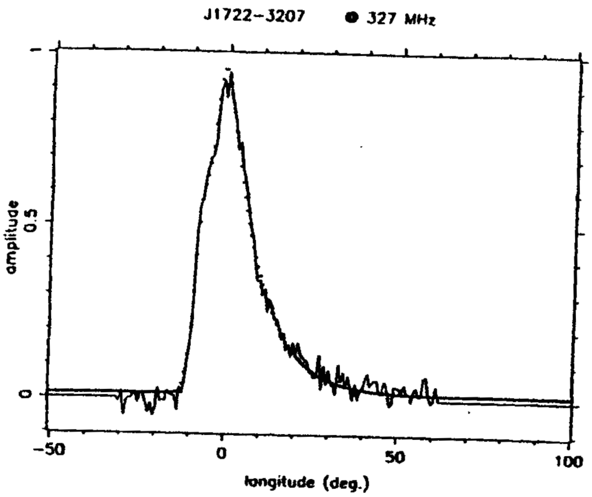
J1722−3207 ● 327 MHz
amplitude
0.5
0
−50
0
50
100
longitude (deg.)

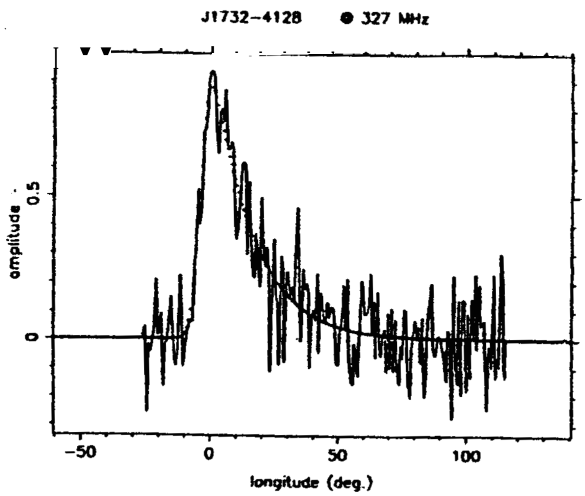
J1732−4128 ● 327 MHz
amplitude
0.5
0
−50
0
50
100
longitude (deg.)

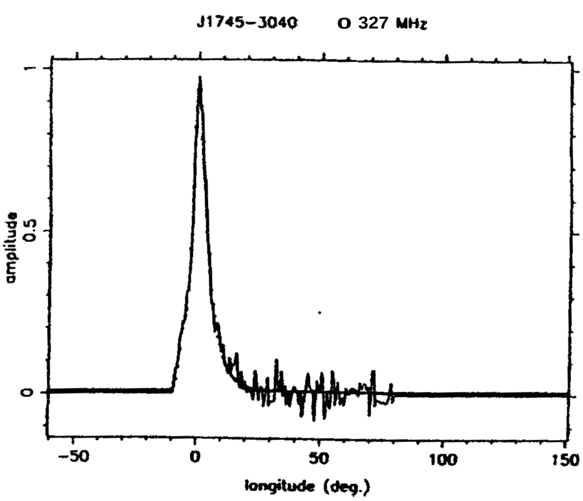
J1745−3040 O 327 MHz
amplitude
1
0.5
0
−50
0
50
100
150
longitude (deg.)

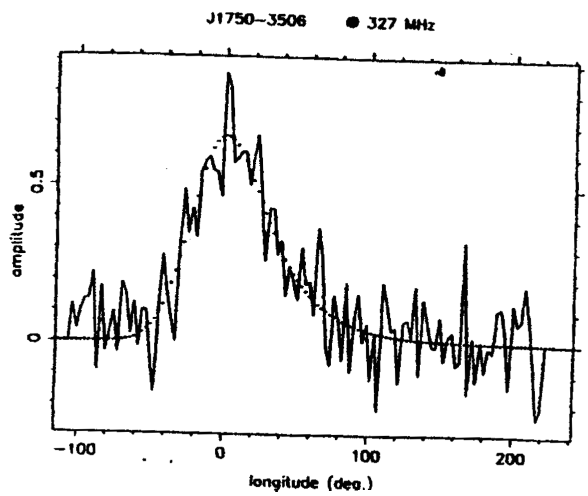
J1750−3506 ● 327 MHz
amplitude
0.5
0
−100
0
100
200
longitude (deg.)

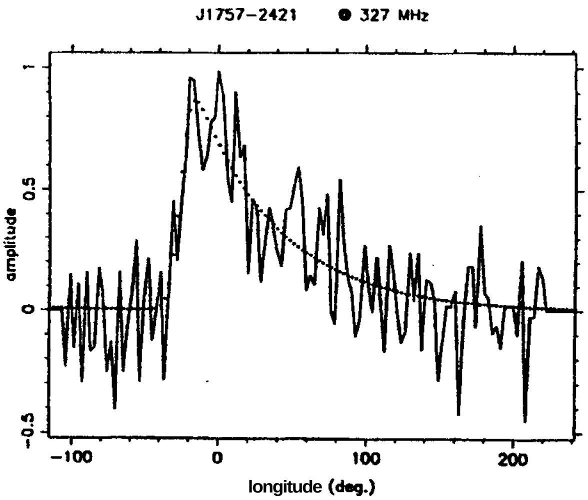
J1757-2421 ● 327 MHz
amplitude
1
0.5
0
-0.5
-100
0
100
200
longitude (deg.)

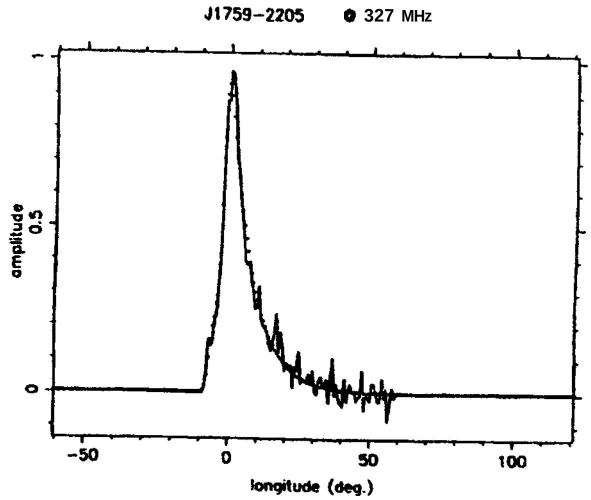
J1759-2205 ● 327 MHz
amplitude
0.5
0
-50
0
50
100
longitude (deg.)

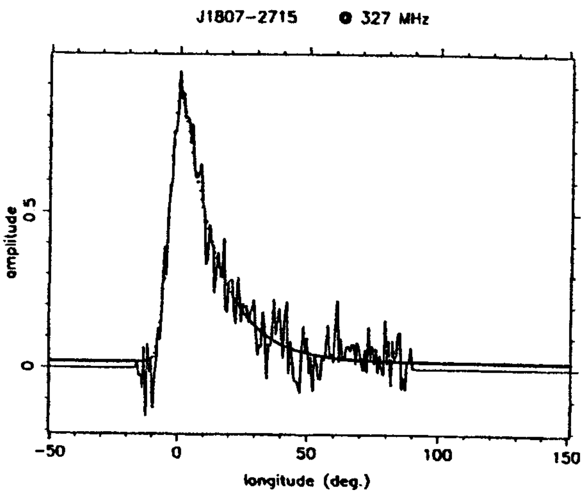
J1807-2715 ● 327 MHz
amplitude
0.5
0
-50
0
50
100
150
longitude (deg.)

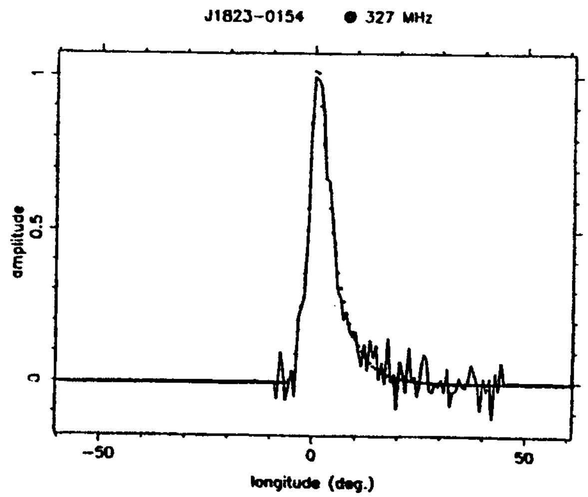
J1823-0154 ● 327 MHz
amplitude
1
0.5
-50
0
50
longitude (deg.)

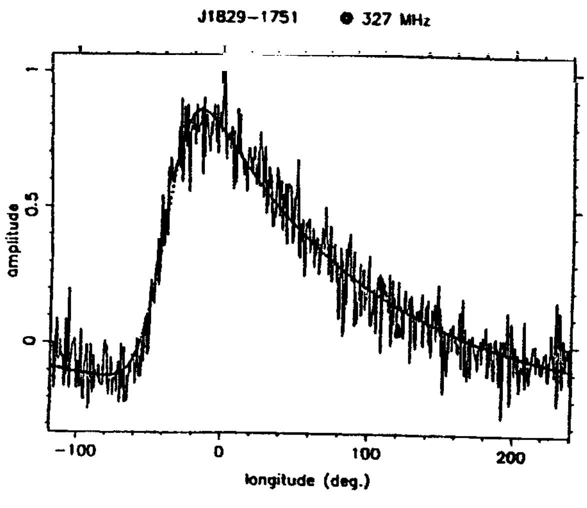
J1829-1751 ● 327 MHz
amplitude
1
0.5
0
-100
0
100
200
longitude (deg.)

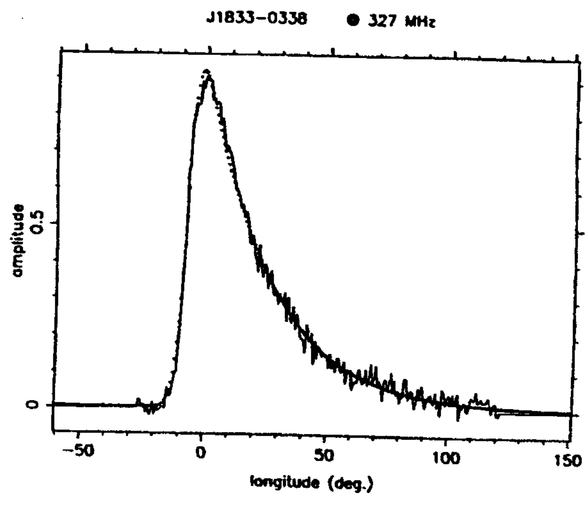
J1833-0338 ● 327 MHz
amplitude
0.5
0
-50
0
50
100
150
longitude (deg.)

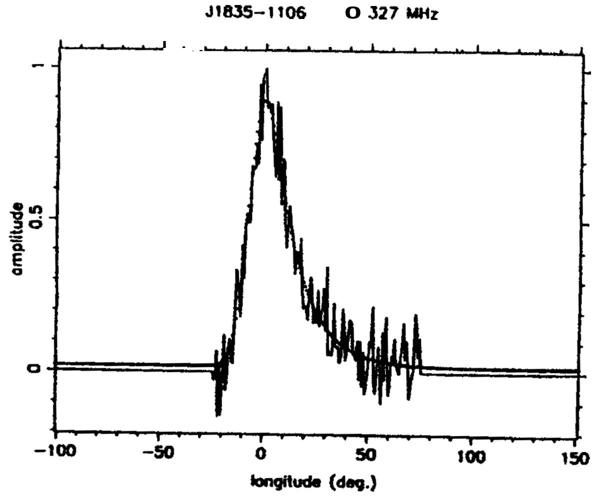
J1835−1106 O 327 MHz
amplitude
0
0.5
1
−100
−50
0
50
100
150
longitude (deg.)

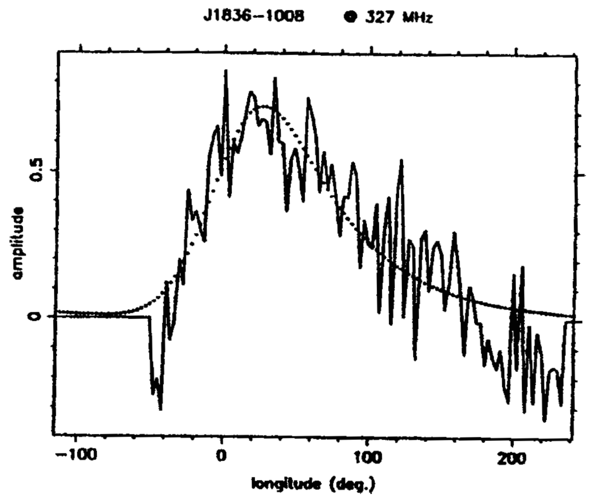
J1836−1008 ● 327 MHz
amplitude
0
0.5
−100
0
100
200
longitude (deg.)

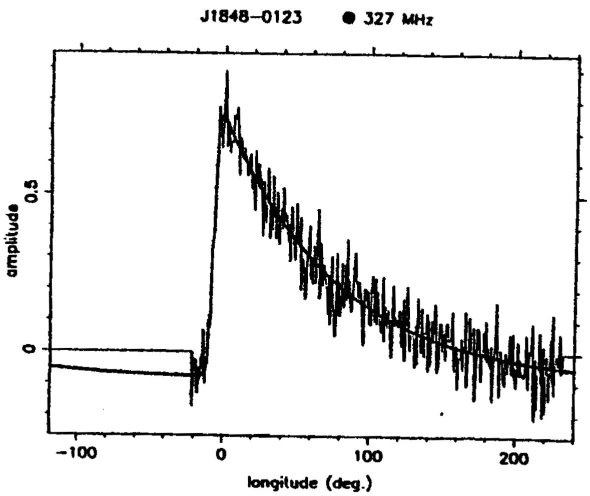
J1848−0123 ● 327 MHz
amplitude
0
0.5
−100
0
100
200
longitude (deg.)

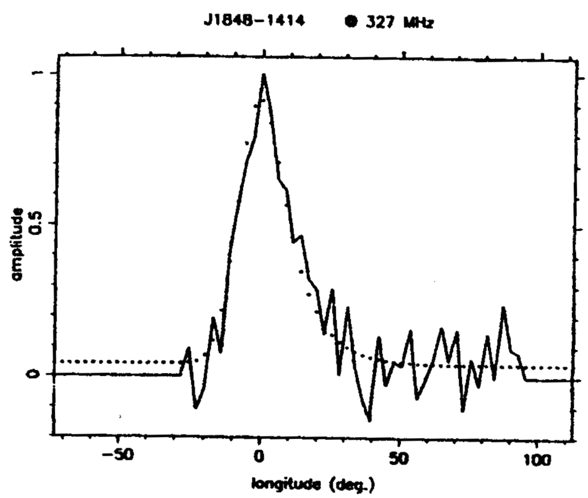
J1848−1414 ● 327 MHz
amplitude
0
0.5
1
−50
0
50
100
longitude (deg.)

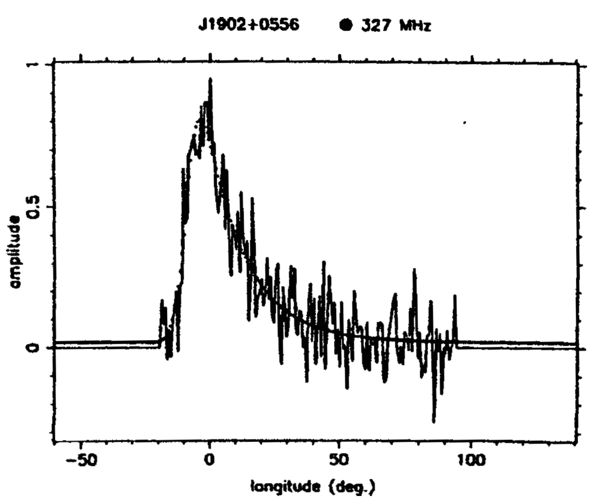
J1902+0556 ● 327 MHz
amplitude
0
0.5
1
−50
0
50
100
longitude (deg.)

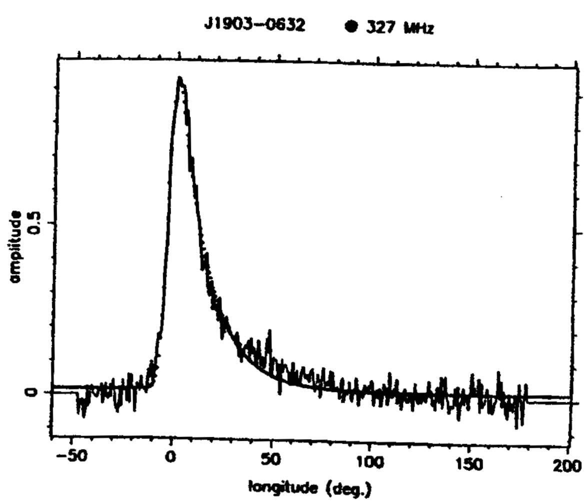
J1903−0632 ● 327 MHz
amplitude
0
0.5
−50
0
50
100
150
200
longitude (deg.)

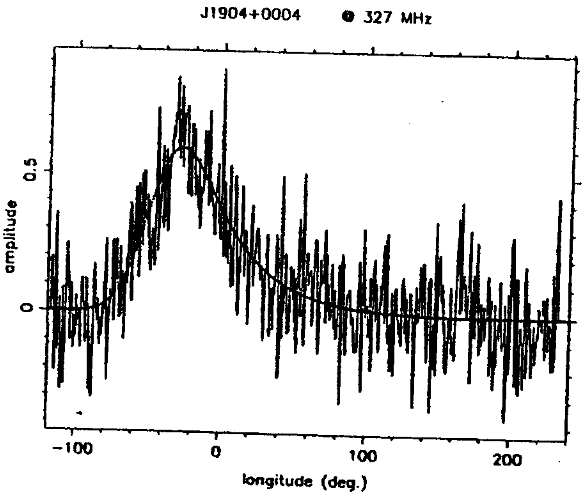
J1904+0004 ● 327 MHz
amplitude
0.5
0
-100
0
100
200
longitude (deg.)

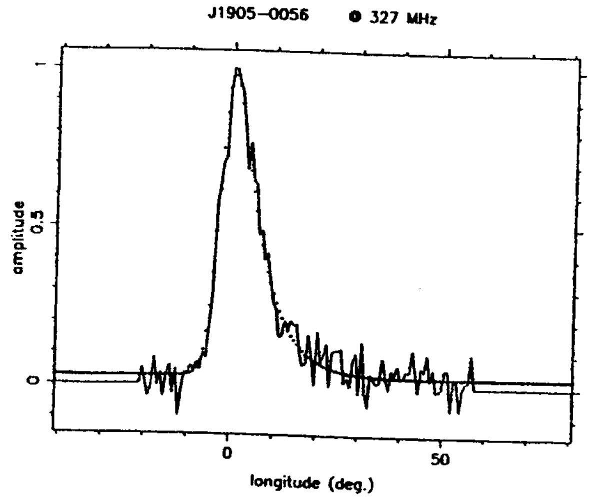
J1905-0056 ● 327 MHz
amplitude
1
0.5
0
0
50
longitude (deg.)

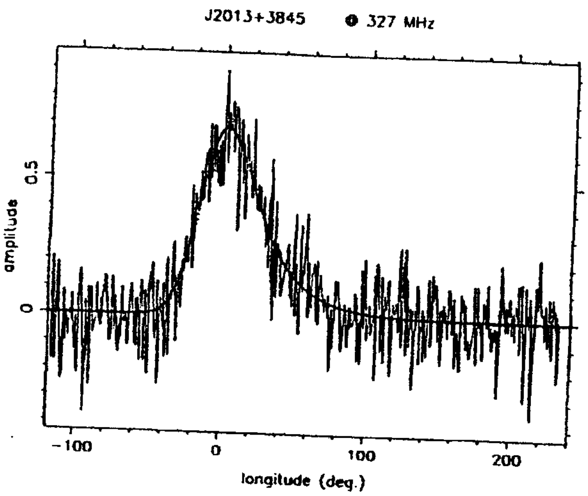
J2013+3845 ● 327 MHz
amplitude
0.5
0
-100
0
100
200
longitude (deg.)

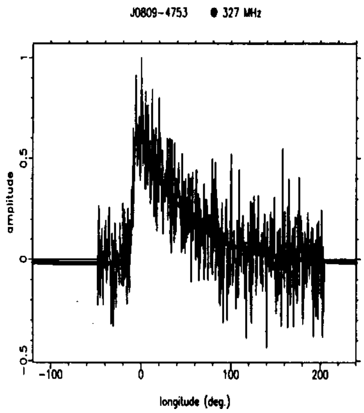
J0809-4753 ● 327 MHz
amplitude
longitude (deg.)

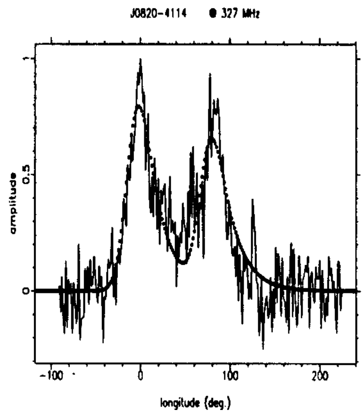
J0820-4114 ● 327 MHz
amplitude
longitude (deg.)

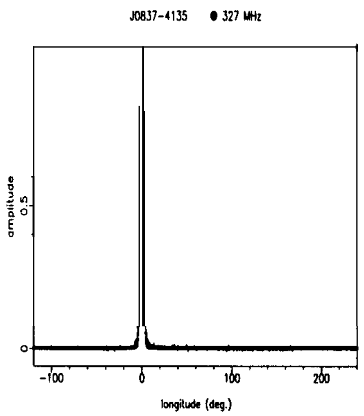
J0837-4135 ● 327 MHz
amplitude
longitude (deg.)

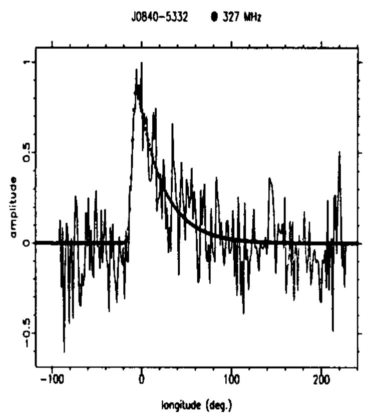
J0840-5332 ● 327 MHz
amplitude
longitude (deg.)

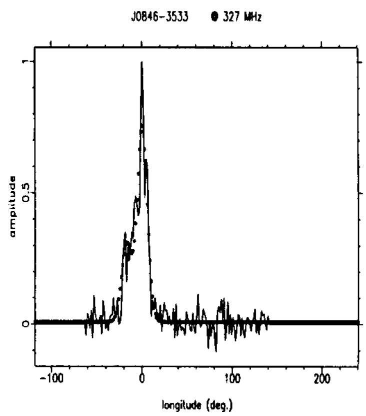
J0846-3533 ● 327 MHz
amplitude
longitude (deg.)

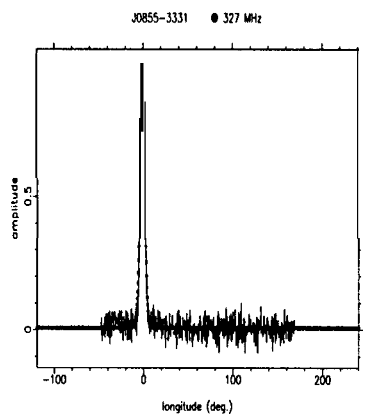
J0855-3331 ● 327 MHz
amplitude
longitude (deg.)

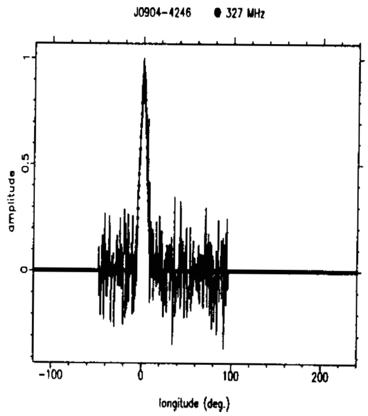
J0904-4246 ● 327 MHz
amplitude
longitude (deg.)

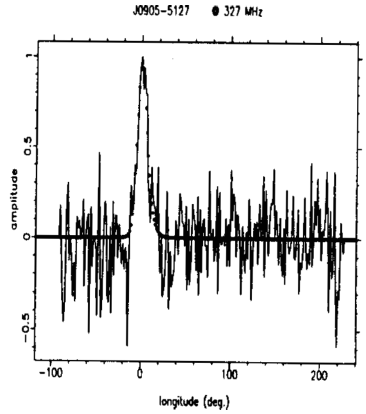
J0905-5127 ● 327 MHz
amplitude
longitude (deg.)

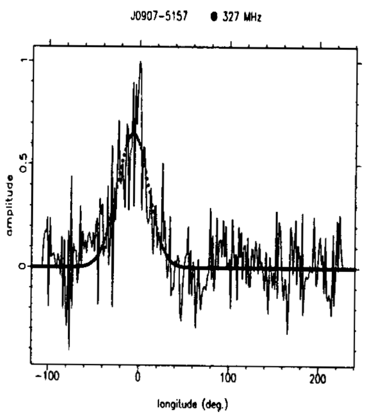
J0907-5157 ● 327 MHz
amplitude
longitude (deg.)

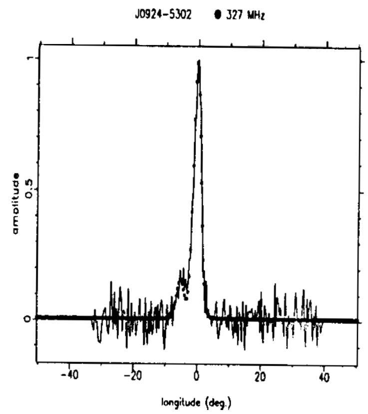
J0924-5302 ● 327 MHz
amplitude
longitude (deg.)

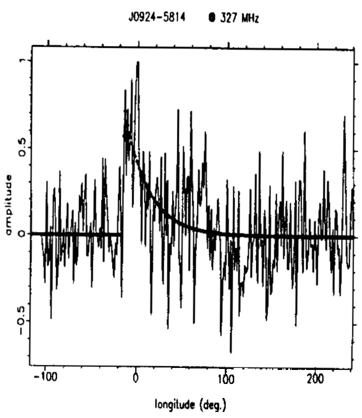
J0924-5814 ● 327 MHz
amplitude
longitude (deg.)

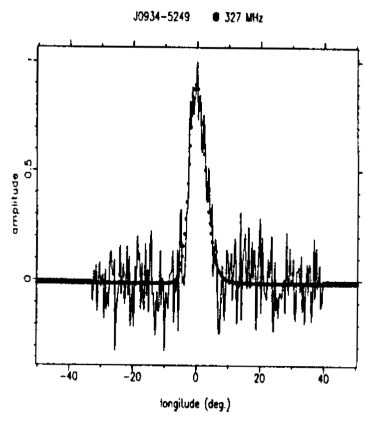
J0934-5249 ● 327 MHz
amplitude
longitude (deg.)

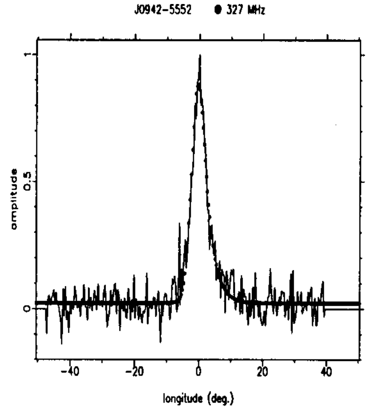
J0942-5552 ● 327 MHz
amplitude
longitude (deg.)

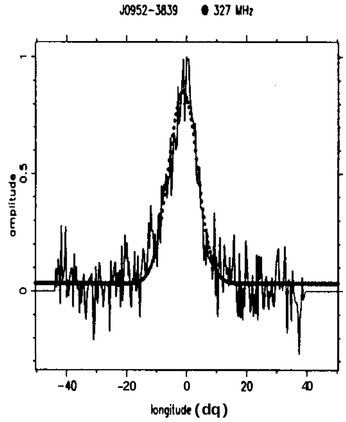
J0952-3839 ● 327 MHz
amplitude
longitude (dq)

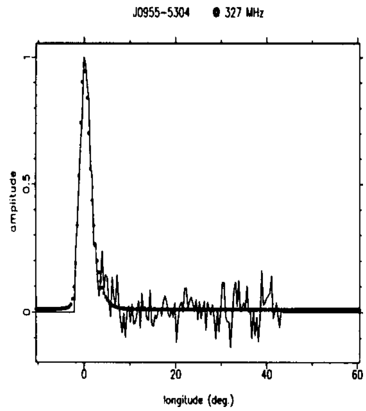
J0955-5304 ● 327 MHz
amplitude
longitude (deg.)

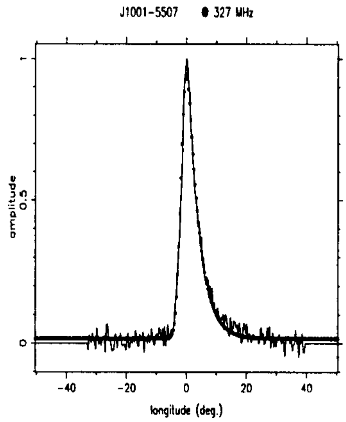
J1001-5507 ● 327 MHz
amplitude
longitude (deg.)

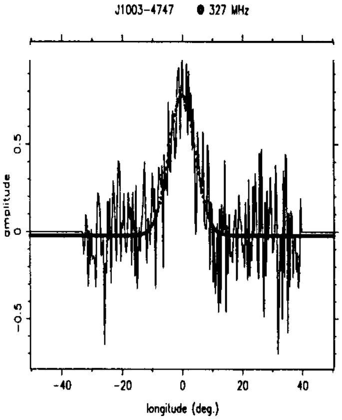
J1003-4747 ● 327 MHz
amplitude
longitude (deg.)

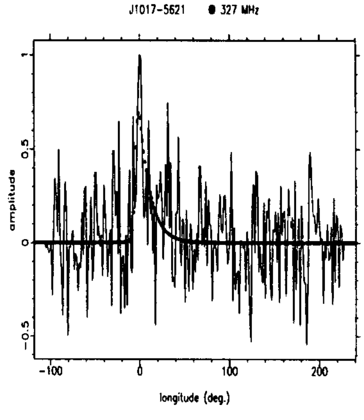
J1017-5621 ● 327 MHz
amplitude
longitude (deg.)

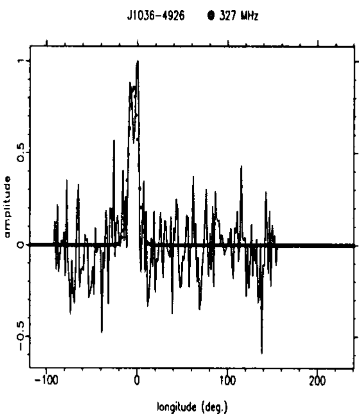
J1036-4926 ● 327 MHz
amplitude
longitude (deg.)

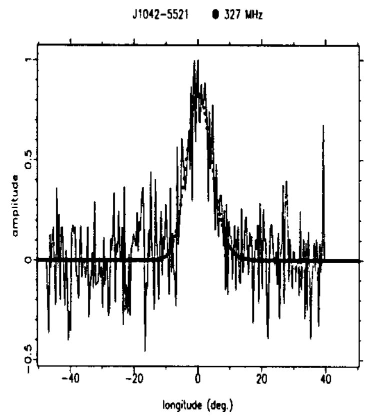
J1042-5521 ● 327 MHz
amplitude
longitude (deg.)

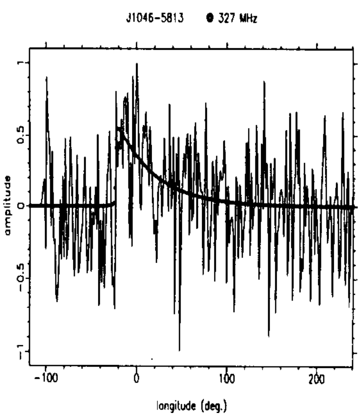
J1046-5813 ● 327 MHz
amplitude
longitude (deg.)

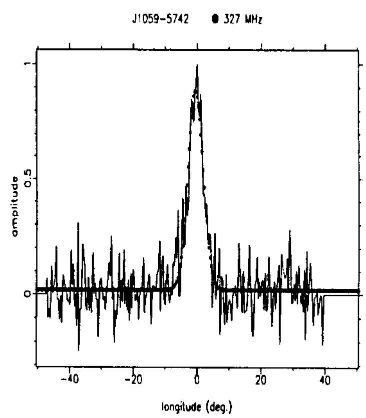
J1059-5742 ● 327 MHz
amplitude
longitude (deg.)